

Supplement of Atmos. Chem. Phys., 20, 1531–1547, 2020
<https://doi.org/10.5194/acp-20-1531-2020-supplement>
© Author(s) 2020. This work is distributed under
the Creative Commons Attribution 4.0 License.



Supplement of

Biomass-burning-derived particles from a wide variety of fuels – Part 1: Properties of primary particles

Crystal D. McClure et al.

Correspondence to: Crystal D. McClure (cdcappa@ucdavis.edu)

The copyright of individual parts of the supplement might differ from the CC BY 4.0 License.

1 1.1 Description of Instrumentation

2 Particle Optical Property Measurements

3 Particle optical properties for PM₁ were measured at 405 nm and 532 nm using the UC Davis
4 Cavity Ringdown-Photoacoustic Spectrometer (CRD-PAS). In the UC Davis CRD-PAS, Light
5 absorption coefficients (b_{abs} ; units = Mm⁻¹) for dry particles are determined using photoacoustic
6 spectroscopy (Lack et al., 2012b). Light extinction coefficients (b_{ext} ; units = Mm⁻¹) for dry (<20%
7 relative humidity) particles are measured at 405 nm and 532 nm via cavity ringdown spectroscopy
8 (Langridge et al., 2011). Humidified light extinction measurements (RH ~85%) are also measured
9 at 532 nm by cavity ringdown spectroscopy. The absorption measurements from the PAS were
10 calibrated relative to the extinction measurement from the CRD using gas-phase O₃ and NO₂ with
11 an estimated accuracy of 5% at 532 nm and 8% at 405 nm. Light absorption and scattering
12 coefficients were also measured at 781 nm using a commercial PASS-3 photoacoustic
13 spectrometer (DMT, Inc.). In the PASS-3, light absorption coefficients are measured by
14 photoacoustic spectroscopy. Light scattering coefficients (b_{sca} ; units = Mm⁻¹) are determined for
15 dry particles with the PASS-3 using reciprocal nephelometry. The absorption measured by the
16 PASS-3 was calibrated relative to the UC Davis PAS using polydisperse fullerene soot and
17 assuming that the absorption Ångstrom exponent was 1.4 (Metcalf et al., 2013). The estimated
18 uncertainty in b_{abs} at 781 nm is 10%.

19 Particle Composition Measurements

20 Refractory black carbon measurement

21 Refractory black carbon (rBC) concentrations and BC-specific particle size distributions were
22 measured using a single particle soot photometer (SP2). The SP2 measures the concentration of
23 rBC within individual rBC-containing particles. Sampled particles pass through a 1064 nm
24 intracavity laser. Absorption of this light by rBC leads to rapid heating of the particles. If heating
25 outweighs conductive cooling the particles will reach a sufficiently high temperature (i.e. their
26 boiling point) that they will incandesce. The intensity of this incandescent light is proportional to
27 the rBC mass of that particle (usually on the order of 0.1 – 10 fg per particle). Size distributions of

28 only the rBC (exclusive of any other internally mixed material) are generated by converting the
29 per particle mass to a volume equivalent diameter ($d_{p,VED}$ here, assuming $\rho_{rBC} = 1.8 \text{ g cm}^{-3}$) and
30 binning the particles by size. The SP2 was calibrated using size-selected fullerene particles (Lot
31 L20W054, Alfa Aesar, Ward Hill, MA, USA).

32 When the number concentration of rBC-containing or non-rBC-containing particles is large,
33 the SP2 may suffer from negative biases in the concentration measurement. This can happen when
34 the SP2 detectors are triggered by one particle and a second passes through the viewing volume
35 during the detection window (typically $\sim 50 \text{ }\mu\text{s}$). Such particle coincidence effects can be
36 minimized by decreasing the sample flowrate into the SP2 to decrease the likelihood that two
37 particles are simultaneously in the viewing volume. Here, the SP2 sample flowrate was varied
38 from 5 sccm to 120 sccm in a step-wise manner over the course of an experiment to deal with the
39 very large dynamic range of concentrations in the mini chamber. The flow rate was increased to
40 maintain an approximately constant particle count rate in the instrument while minimizing the
41 influence of particle coincidence. Inspection of individual particle detection events indicates that
42 particle coincidence was generally avoided.

43 The SP2 data were processed using the SP2 Toolkit from the Paul Scherer Institute (PSI),
44 developed by Martin Gysel. The SP2 size-dependent counting efficiency was determined by
45 simultaneously measuring the concentration of the calibration particles with a mixing condensation
46 particle counter (BMI Model 2002). The particle counting efficiency was found to be unity for
47 particles with $d_{p,VED} > 100 \text{ nm}$. The SP2 used in this study measured particles over the size range
48 $90 \leq d_{p,VED} \leq 822$. Below the lower size limit, the detection efficiency falls off rapidly due, in part,
49 to the large surface area-to-volume (SA-to-V) ratio of these particles. When the SA-to-V ratio is
50 sufficiently large conductive cooling competes effectively with the radiative heating from the laser
51 and the particles do not emit enough incandescent light at short enough wavelengths to trigger
52 detection. Above the upper size limit, the incandescence level is sufficient to saturate the detector,
53 leading to an underestimate in particle mass. All SP2 mass concentration measurements were
54 corrected for the missing mass contained in particles below the lower and upper size limit, using a
55 multi-mode fitting approach.

56 The observed campaign average distribution mode peak is around 150 nm. The observed
57 distributions (1 min averages) were fit to a four-mode log-normal distribution to estimate and

58 correct for the rBC outside of the SP2 detection window, i.e. for rBC “missing mass”. The average
59 ratio between the observed rBC concentration and the total estimated from fitting was 0.83 ± 0.06
60 (1σ). There was some experiment-to-experiment and time-dependent variability in the missing
61 mass fraction that is accounted for by fitting the observations at 1 min time resolution. This
62 approach follows that of Zhang et al. (2016). While a single mode fit provides a reasonably
63 representation of the overall campaign average distribution, inspection of the individual
64 distributions across the experiments indicates that a multi-mode fitting approach provides a
65 substantially more robust description of the observed size distribution, especially as particle aging
66 proceeds.

67 Composition and concentration of NR-PM

68 The concentration of non-refractory particulate matter (NR-PM) species in PM_{10} were measured
69 using a high-resolution time-of-flight aerosol mass spectrometer (HR-ToF-AMS, henceforth HR-
70 AMS) (Canagaratna et al., 2007) during both the Fresno and Fontana studies, as discussed in detail
71 by (Lim et al., 2019). The NR-PM components are functionally defined as those materials that
72 evaporate rapidly after impaction onto a heated surface *in vacuo* at ~ 600 °C. The NR-PM
73 components characterized include particulate sulfate, nitrate, ammonium, chloride and organic
74 matter. The data were processed using the PIKA toolkit in IGOR (Wavemetrics, Inc.). The
75 collection efficiency (CE) of the HR-AMS was determined by comparison with size distributions
76 measured using the scanning electrical mobility spectrometer (SEMS). The collection efficiency
77 differed between primary and secondary and secondary particles and was found to co-vary with
78 the volatility of the organic aerosol. The variation in the CE was empirically accounted for, as
79 discussed in (Lim et al., 2019). The estimated uncertainty for the HR-AMS measurements is $\pm 30\%$,
80 although the precision is much better than this.

81 Particulate nitrated organics characterization

82 The concentration of nitrated organic functional groups (ON_f) is determined from the HR-AMS
83 measurements. Kiendler-Scharr et al. (2016) showed that the fraction of total nitrate measured by
84 the HR-AMS that derives from organic nitrate functional groups (f_{ON-N}) relates to the measured
85 $[NO_2^+]/[NO^+]$ ratio (R_{meas}):

$$f_{ON-N} = \frac{(1+R_{ON}) \cdot (R_{meas} - R_{calib})}{(1+R_{meas}) \cdot (R_{ON} - R_{calib})} \quad (S1)$$

87 where $R_{ON} = 0.1$ and R_{calib} is an instrument-specific factor determined from calibration with
 88 NH_4NO_3 and here equaling 0.45. The Kiendler-Scharr et al. (2016) approach focused on the
 89 behavior of organic nitrates. We assume here that nitro-organics behave similarly and thus that
 90 ON_f encompasses contributions from both nitrate and nitro functional groups. Equation S1 is
 91 thought reliable when the $f_{ON-N} > 0.15$ (Bruns et al., 2010). The average f_{ON-N} for the FIREX
 92 measurements is 0.74 ± 0.24 (1σ). The concentration of particulate ON functional groups is then
 93 $[ON_f] = f_{ON-N} [NO_3^-]$. Note that this includes only the mass of the functional group; the total mass
 94 concentration of the ON species (including the carbon backbone) can be estimated by multiplying
 95 the ON_f concentration by the ratio between an assumed MW for the ON species and that for the
 96 nitrate functional group. We assume that ON species have a MW = 200 amu, and thus $[ON] =$
 97 $3.22 [ON_f]$. If the ON signal is dominated by nitro functional groups, rather than nitrate, then the
 98 estimated $[ON]$ is a lower limit.

99 Composition and concentration of BC-containing particles

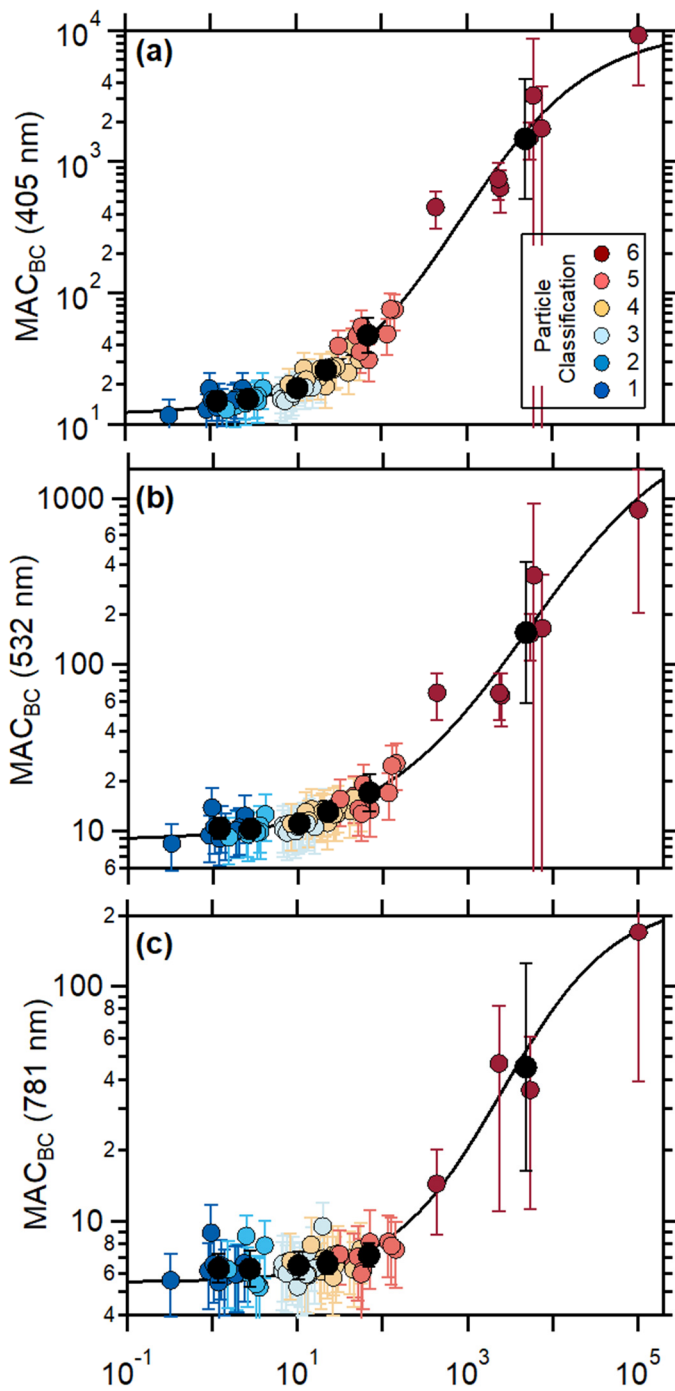
100 The concentrations and composition of only BC-containing particles were determined using a
 101 soot particle aerosol mass spectrometer (SP-AMS) (Onasch et al., 2012). In the SP-AMS, a focused
 102 particle beam is intersected with an intra-cavity Nd:YAG laser operating at 1064 nm. Particles
 103 containing BC are rapidly heated by the laser, leading to evaporation of both the NR-PM materials
 104 and the refractory BC. In these studies, the standard HR-AMS tungsten vaporizer was removed so
 105 that particles that do not contain BC are not vaporized and are therefore not detected. Thus, the
 106 SP-AMS is specific to BC-containing particles, as operated here. In addition to BC, the SP-AMS
 107 measures the internally mixed particulate inorganic (sulfate, nitrate, ammonium, and chloride) and
 108 organic mass loading. The NR-PM species that are associated with BC will be distinguished from
 109 the bulk average NR-PM species (from the HR-AMS) using the subscript BC (i.e. NR-PM_{rBC}).
 110 The SP-AMS particle detection efficiency is determined in large part by the extent of overlap
 111 between the particle and laser beam. Particles were sampled through a PM₁ aerodynamic lens, with
 112 particles measured down to ~40 nm vacuum aerodynamic diameter. The SP-AMS detection
 113 efficiency was determined by referencing the rBC concentration measured by the SP-AMS to that
 114 measured by the SP2, as in (Collier et al., 2018). The SP-AMS/SP2 ratio depended on the ratio

115 between the NR-PM_{BC} and BC, with the NR-PM/rBC ratio decreasing as the SP-AMS/SP2 ratio
116 increases. However, throughout this work we use only the [NR-PM]_{rBC}/[rBC] or [OA]_{rBC}/[rBC]
117 ratios, which are not dependent on the absolute instrument calibration, but only the relative
118 detection efficiency of these species. The coating-to-core mass ratio for both campaigns is
119 calculated directly from the SP-AMS measurements as $R_{BC} = [\text{NR-PM}]_{BC}/[\text{BC}]$.

120 **Gas Composition Measurements**

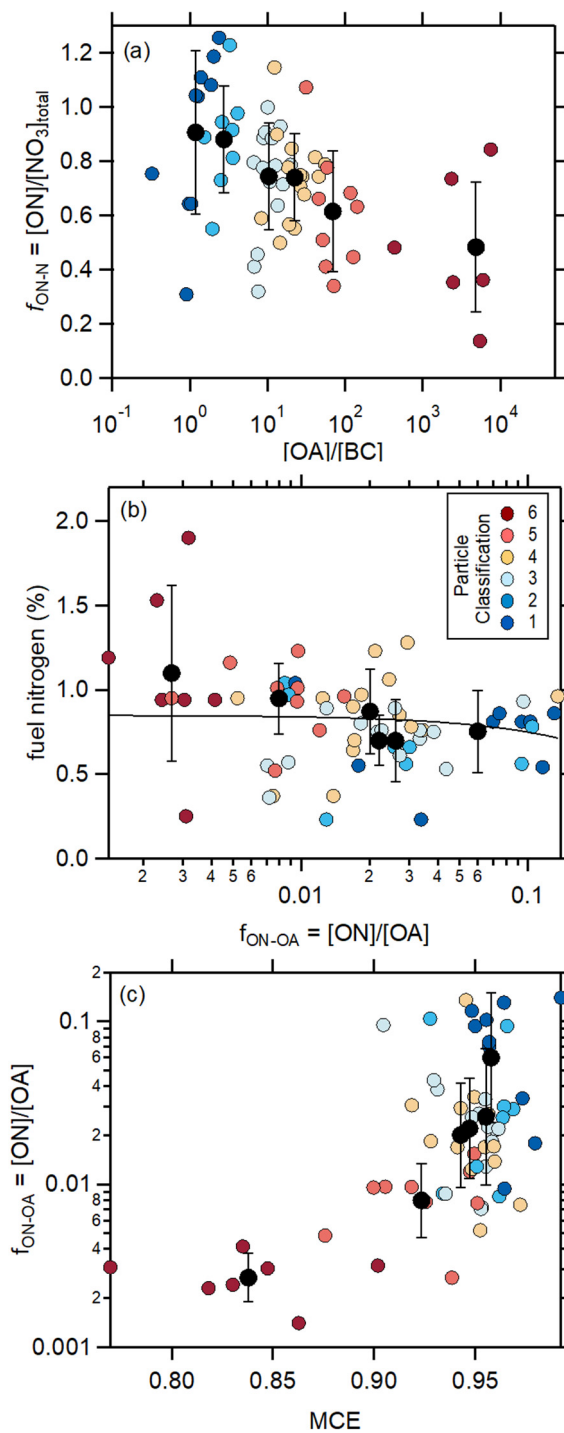
121 The concentrations of select gas-phase non-methane organic gases (NMOG) and some
122 inorganic species (e.g. HONO) were measured using H₃O⁺ and I⁻ chemical ionization mass
123 spectrometers (CIMS), that included high-resolution time-of-flight mass spectrometers. Only the
124 measurements from the PTR-TOF-MS, operated by the National Oceanic and Atmospheric
125 Administration, are used here. The PTR-TOF-MS measurements are described in detail in (Koss
126 et al., 2018) and (Sekimoto et al., 2018). In addition to the NMOG measurements, other inorganic
127 gases (O₃, CO, CO₂, SO₂) were measured using commercial instrumentation.

128



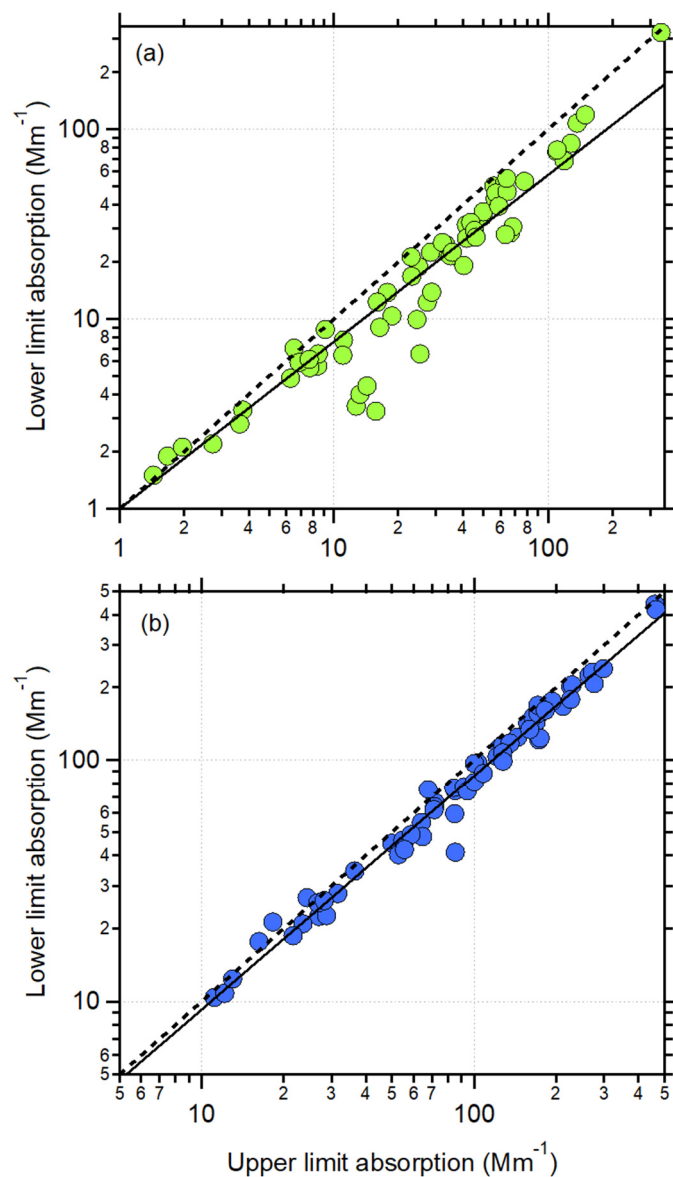
130

131 **Figure S1.** Relationship between the observed ambient particle MAC_{BC} and the total particle
 132 $[OA]/[rBC]$ at (a) 405 nm, (b) 532 nm, and (c) 781 nm. Individual points colored by Class (see
 133 text) and class averages as black circles.



134

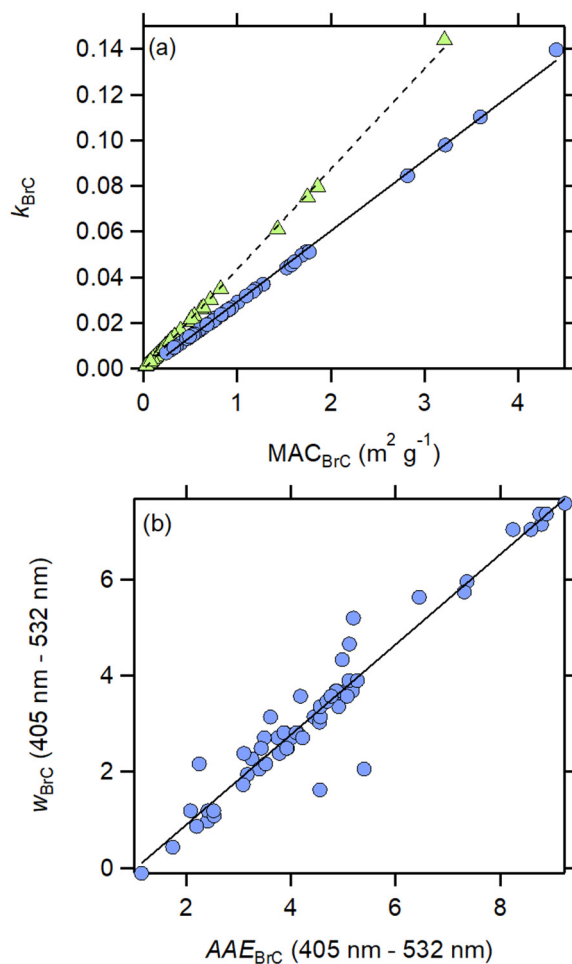
135 **Figure S2.** (a) Relationship between fuel nitrogen and the fraction of OA that is organic nitrate,
 136 $f_{\text{ON-N}}$. There is no correlation between the two. (b) Relationship between $f_{\text{ON-OA}}$ and the modified
 137 combustion efficiency, MCE. Results for individual burns are shown as points colored by the
 138 particle Class, and Class average values are shown as black circles. Uncertainties on the Class
 139 averages are 1σ based on measurement variability.



140

141 **Figure S3.** The derived lower limit brown carbon absorption versus the upper limit brown carbon
 142 absorption at (a) 532 nm and (b) 405 nm. The lower limit estimate for BrC absorption accounts for
 143 the potential influence of coating-induced enhancements. The dashed line is the one-to-one line
 144 and the solid line is a linear fit with slopes equaling 0.88 at 532 nm and 0.97 at 405 nm.

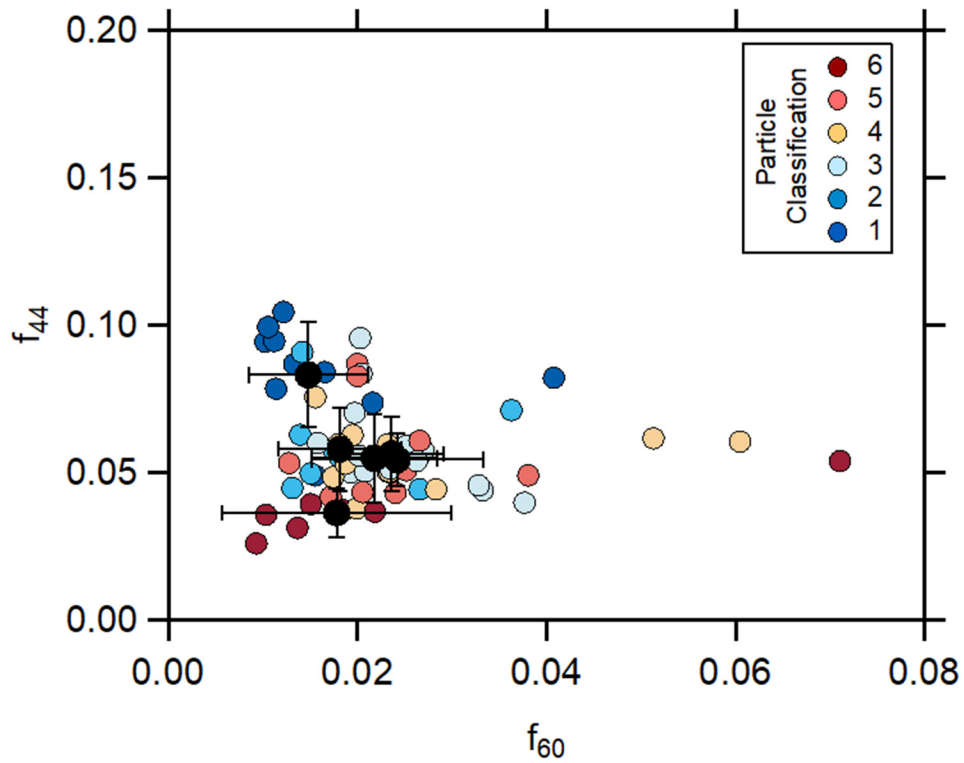
145



146

147 **Figure S4.** (a) Relationship between the imaginary refractive index for BrC, k_{BrC} , at 405 nm (blue
 148 circles) and the observed MAC_{BrC} at 405 nm or at 532 nm (green triangles). Lines are linear fits to
 149 the observations. (b) Relationship between the wavelength dependence of k_{BrC} , w_{BrC} , determined
 150 for the 405 nm – 532 nm pair, and the AAE_{BrC} for the same wavelengths.

151



153

154 **Figure S5.** The relationship between the fractional abundance of the $m/z = 44$ (f_{44}) and $m/z = 60$
155 (f_{60}) ions from organic aerosol. Points are colored by particle class for individual burns, and the
156 class averages shown in black.

157

158 **Table S1.** Fuels combusted. Further details regarding fuel properties are available at the NOAA
159 data repository, in particular in the summary spreadsheet
160 ([https://esrl.noaa.gov/csd/groups/csd7/measurements/2016firex/FireLab/DataDownload/FIREX_](https://esrl.noaa.gov/csd/groups/csd7/measurements/2016firex/FireLab/DataDownload/FIREX_BurnListComplete_V5.xlsx)
161 [BurnListComplete_V5.xlsx](https://esrl.noaa.gov/csd/groups/csd7/measurements/2016firex/FireLab/DataDownload/FIREX_BurnListComplete_V5.xlsx); access date 04 February 2019)

Fuel Type

Bear Grass
Building Material - Untreated Wood
Ceanothos
Chapparral (canopy)
Chamise
Manzanita
Douglas Fir (litter, canopy, mixture, rotten log)
Dung
Engelmann spruce (canopy, mixture, duff)
Excelsior (wood wool)
Jeffrey Pine (duff)
Juniper (canopy)
Loblolly pine (litter)
Lodgepole (canopy, litter, mixture)
Peat
Ponderosa pine (litter, canopy, mixture, rotten log)
Rice Straw, Arkansas
Sage
Sage Brush
Subalpine fir (canopy, litter, mix, duff)

162

163

164 **Table S2.** Fit coefficients for the various fits performed, organized by fit type (e.g. sigmoidal,
 165 power law, linear, exponential). Note: continues on second page.

y	x	c ₁	c ₂	c ₃	c ₄	r ²
$y = c_1 + \frac{c_2}{1 + \frac{\exp(c_3 - x)}{c_4}}$						
SSA _{405nm}	log([OA]/[BC])	0.03	0.93	0.444	0.579	
SSA _{532nm}	log([OA]/[BC])	0.085	0.91	0.623	0.520	
SSA _{781nm}	log([OA]/[BC])	0.10	0.90	0.700	0.538	
AAE ₄₀₅₋₅₃₂	log([OA]/[BC])	1.25	7.81	2.298	0.554	
log(MAC _{BC,405nm})	log([OA]/[BC])	1.072	2.94	2.914	0.765	
log(MAC _{BC,532nm})	log([OA]/[BC])	0.94	2.56	3.721	0.900	
log(MAC _{BC,781nm})	log([OA]/[BC])	0.74	1.62	3.411	0.655	
log(<i>f</i> _{OA,int})	log([OA]/[BC])	0	-2.43	1.477	0.987	
log(<i>R</i> _{OA,BC})	log([OA]/[BC])	-1.76	3.70	0.462	1.823	
log(MAC _{BrC,405nm})	log([OA]/[BC])	1.072	-1.519	0.053	0.732	
AAE _{405-532nm}	MCE	9.124	-7.476	0.884	0.0236	
AAE _{405-532nm}	MCE*	9.723	-13.142	0.932	0.0452	
log(MAC _{BC,405nm})	MCE	3.523	-2.251	0.874	0.0198	
log(MAC _{BC,405nm})	MCE*	4.949	-5.073	0.882	0.0705	
log([OA]/[BC])	MCE*	4.030	-39.57	1.072	0.0500	
$y = c_1 + c_2 \cdot x^{c_3}$						
SSA _{405nm}	MCE	0.954	-0.880	22.76		
SSA _{405nm}	MCE*	0.939	-26.34	88.29		
log([OA]/[BC])	MCE	7.952	-8.272	3.351		
$y = c_1 \cdot x + c_2$						
<i>f</i> ₄₄	log([OA]/[BC])	-0.0097	0.0686			0.33
O:C	log([OA]/[BC])	-0.0345	0.407			0.17
H:C	log([OA]/[BC])	0.0228	1.737			0.27
log(MAC _{BrC,405nm})	log(<i>f</i> _{ON-OA})	0.322	0.446			0.33
log(MAC _{BrC,405nm})	log(<i>f</i> _{ON-OA})*	0.856	0.538			0.81
log(MAC _{BrC,405nm})	<i>f</i> ₆₀ / <i>f</i> ₄₄	-0.396	0.043			0.11
log(MAC _{BrC,405nm})	<i>f</i> ₆₀ / <i>f</i> ₄₄ *	-2.242	0.803			0.96
log([ON]/[OA])	log([OA]/[BC])	-1.342	-0.320			0.47
log([ON]/[OA])	log([OA]/[BC])*	-1.342	-0.320			0.47
<i>k</i> _{BrC,405nm}	MAC _{BrC,405nm}	0.03104	-0.00177			0.99
<i>k</i> _{BrC,532nm}	MAC _{BrC,532nm}	0.0440	-0.00048			0.99

y	x	c₁	c₂	c₃	c₄	r²
W _{BrC,405-532}	AAE _{BrC,405-532}	0.938	-0.976			0.96
		$y = c_1 + c_2 \cdot \exp(-c_3 \cdot x)$				
MFR _{OA}	log([OA]/[BC])	0.00175	0.1760	0.8520		0.157

* Fits were performed to the Class averages, rather than to the individual burns.

166

167

168 **Table S3.** Literature imaginary refractive index and *MAC* values for biomass burning derived
 169 brown carbon.

	λ , nm	k_{BBOA}	MAC_{BBOA} $m^2 g^{-1}$	Optical Measurement	Aerosol type sampled	Sampling Location or note	Literature
Laboratory	550	0.02-0.06		Aethalometer	Oak burning POA	-	(Saleh et al., 2013)
	550	0.015-0.04		Aethalometer	Pocosin Pine burning POA	-	(Saleh et al., 2013)
	550	0.0055- 0.022		Aethalometer	Galberry burning POA	-	(Saleh et al., 2013)
	400	0.038	1.1	UV/Vis (filter methanol extracts)	Pine/Oak wood burning	-	(Chen and Bond, 2010)
	405	0.015		Photo-Acoustic Spectrometer	Tar balls from Ponderosa Pine Duff burning	-	(Chakrabarty et al., 2010)
	405	0.0076		Photo-Acoustic Spectrometer	Tar balls from Alaskan Duff burning	-	(Chakrabarty et al., 2010)
	550		0.8-3.2	CLAP	Tar balls from liquid tar (turkey oak)	-	(Hoffer et al., 2016)
	405	0.01	0.35	Photo-Acoustic Spectrometer	Alaskan Peat	-	(Sumlin et al., 2017)
	355, 405, 532, 1064	0.012, 0.0065, 0.0024, 0.0023		Photo-Acoustic Spectrometer	Alaskan & Indonesian Peat	central values reported here	(Sumlin et al., 2018)
	600/400 ratio		0.04	Water soluble organic carbon	Florida peat	Ratio between wavelengths reported	(Sengupta et al., 2018)
Ambient	404	0.01	1.0-1.1	Photo-Acoustic Spectrometer	Wild fire, near- source emission	Four Mile Canyon, Colorado	(Lack et al., 2012a)
	470		1.01	Aethalometer	Biomass burning influenced	Beijing, China	(Yang et al., 2009)
	400	0.112	2.9	Filter transmission	Wood burning and biomass smoke aerosols	Savanna	(Kirchstetter et al., 2004)
	532	0.0016- 0.0019	0.029- 0.031	Photo-Acoustic Spectrometer	HULIS from biomass burning aerosols	Amazon basin	(Hoffer et al., 2006)
	Broadband	0.05-0.07		Airborne lidar	Upwind of forest fires	Northern Canada	(Wandinger et al., 2002)
	Broadband	0.07±0.03/ 0.04±0.01		White light optical particle counter	Open fire/ Smoldering phase	Urban Rehovot, Israel	(Adler et al., 2011)
	405	0.037	0.79 or 1.22	Photo-Acoustic Spectrometer	Residential biomass burning influenced	Fresno, CA	(Zhang et al., 2016)
	405		0.84	Photo-Acoustic Spectrometer	Residential biomass burning influenced	Fresno, CA	(Cappa et al., 2019)
	405		2.3	Aethalometer	Biomass burning influenced	Guangzhou, China	(Qin et al., 2018)
	365		0.32	Water soluble organic carbon	Plume intercept – closest point to fire	Western US	(Forrister et al., 2015)
365		1.35	Water soluble organic carbon	Regional biomass burning	SE US	(Washenfelder et al., 2015)	

405	0.037		Water soluble organic carbon	Regional	Kanpur, India	(Shamjad et al., 2016)
405		0.7-1.3	Water soluble organic carbon	Bonfire festival	Rehovot, Israel	(Bluvshstein et al., 2017)
405		0.6	Methanol soluble organic carbon	Prescribed burn	NW US	(Xie et al., 2017)
400, 600, 800	0.31, 0.26, 0.22		Electron loss	Asian outflow	Downwind of Asia	(Alexander et al., 2008)
800/400 ratio		0.26	Methanol soluble organic carbon	Ambient particles (ratio between wavelengths reported)	Athens, Georgia	(Phillips and Smith, 2017)
400, 550, 700	0.112, 0.030, 0.001		Acetone treatment + attenuation	African biomass burning	Southern Africa	(Kirchstetter et al., 2004)

170

171

172 1.3 Supplemental References

173 Adler, G., Flores, J. M., Abo Riziq, A., Borrmann, S., and Rudich, Y.: Chemical, physical, and
 174 optical evolution of biomass burning aerosols: a case study, *Atmos. Chem. Phys.*, 11, 1491-1503,
 175 <https://doi.org/10.5194/acp-11-1491-2011>, 2011.

176 Alexander, D. T. L., Crozier, P. A., and Anderson, J. R.: Brown Carbon Spheres in East Asian
 177 Outflow and Their Optical Properties, *Science*, 321, 833-836,
 178 <https://doi.org/10.1126/science.1155296>, 2008.

179 Bluvshstein, N., Lin, P., Flores, J. M., Segev, L., Mazar, Y., Tas, E., Snider, G., Weagle, C., Brown,
 180 S. S., Laskin, A., and Rudich, Y.: Broadband optical properties of biomass-burning aerosol and
 181 identification of brown carbon chromophores, *Journal of Geophysical Research: Atmospheres*,
 182 122, 5441-5456, <https://doi.org/doi:10.1002/2016JD026230>, 2017.

183 Bruns, E. A., Perraud, V., Zelenyuk, A., Ezell, M. J., Johnson, S. N., Yu, Y., Imre, D., Finlayson-
 184 Pitts, B. J., and Alexander, M. L.: Comparison of FTIR and Particle Mass Spectrometry for the
 185 Measurement of Particulate Organic Nitrates, *Environmental Science & Technology*, 44, 1056-
 186 1061, <https://doi.org/10.1021/es9029864>, 2010.

187 Canagaratna, M. R., Jayne, J. T., Jimenez, J. L., Allan, J. D., Alfarra, M. R., Zhang, Q., Onasch,
 188 T. B., Drewnick, F., Coe, H., Middlebrook, A., Delia, A., Williams, L. R., Trimborn, A. M.,
 189 Northway, M. J., DeCarlo, P. F., Kolb, C. E., Davidovits, P., and Worsnop, D. R.: Chemical and
 190 microphysical characterization of ambient aerosols with the Aerodyne aerosol mass spectrometer,
 191 *Mass Spectrometry Reviews*, 26, 185-222, <https://doi.org/10.1002/mas.20115>, 2007.

192 Cappa, C. D., Zhang, X., Russell, L. M., Collier, S., Lee, A. K. Y., Chen, C.-L., Betha, R., Chen,
 193 S., Liu, J., Price, D. J., Sanchez, K. J., McMeeking, G., Williams, L. R., Onasch, T. B., Worsnop,
 194 D. R., Abbatt, J., and Zhang, Q.: Light absorption by ambient black and brown carbon and its
 195 dependence on black carbon coating state for two California, USA cities in winter and summer,
 196 *Journal of Geophysical Research-Atmospheres*, <https://doi.org/10.1029/2018JD029501>, 2019.

197 Chakrabarty, R. K., Moosmüller, H., Chen, L. W. A., Lewis, K., Arnott, W. P., Mazzoleni, C.,
198 Dubey, M. K., Wold, C. E., Hao, W. M., and Kreidenweis, S. M.: Brown carbon in tar balls from
199 smoldering biomass combustion, *Atmospheric Chemistry and Physics*, 10, 6363-6370,
200 <https://doi.org/10.5194/acp-10-6363-2010>, 2010.

201 Chen, Y., and Bond, T. C.: Light absorption by organic carbon from wood combustion, *Atmos.*
202 *Chem. Phys.*, 10, 1773-1787, <https://doi.org/10.5194/acp-10-1773-2010>, 2010.

203 Collier, S., Williams, L. R., Onasch, T. B., Cappa, C. D., Zhang, X., Russell, L. M., Chen, C.-L.,
204 Sanchez, K. J., Worsnop, D. R., and Zhang, Q.: Influence of emissions and aqueous processing on
205 particles containing black carbon in a polluted urban environment: Insights from a soot particle –
206 aerosol mass spectrometer, *Journal of Geophysical Research-Atmospheres*, 123, 6648-6666,
207 <https://doi.org/10.1002/2017JD027851>, 2018.

208 Forrister, H., Liu, J., Scheuer, E., Dibb, J., Ziemba, L., Thornhill, K. L., Anderson, B., Diskin, G.,
209 Perring, A. E., Schwarz, J. P., Campuzano-Jost, P., Day, D. A., Palm, B. B., Jimenez, J. L., Nenes,
210 A., and Weber, R. J.: Evolution of brown carbon in wildfire plumes, *Geophysical Research Letters*,
211 42, 4623-4630, <https://doi.org/10.1002/2015GL063897>, 2015.

212 Hoffer, A., Gelencser, A., Guyon, P., Kiss, G., Schmid, O., Frank, G. P., Artaxo, P., and Andreae,
213 M. O.: Optical properties of humic-like substances (HULIS) in biomass-burning aerosols,
214 *Atmospheric Chemistry and Physics*, 6, 3563-3570, <https://doi.org/10.5194/acp-6-3563-2006>,
215 2006.

216 Hoffer, A., Tóth, A., Nyirő-Kósa, I., Pósfai, M., and Gelencsér, A.: Light absorption properties of
217 laboratory-generated tar ball particles, *Atmos. Chem. Phys.*, 16, 239-246,
218 <https://doi.org/10.5194/acp-16-239-2016>, 2016.

219 Kiendler-Scharr, A., Mensah, A. A., Friese, E., Topping, D., Nemitz, E., Prevot, A. S. H., Äijälä,
220 M., Allan, J., Canonaco, F., Canagaratna, M., Carbone, S., Crippa, M., Dall'Osto, M., Day, D. A.,
221 De Carlo, P., Di Marco, C. F., Elbern, H., Eriksson, A., Freney, E., Hao, L., Herrmann, H.,
222 Hildebrandt, L., Hillamo, R., Jimenez, J. L., Laaksonen, A., McFiggans, G., Mohr, C., O'Dowd,
223 C., Otjes, R., Ovadnevaite, J., Pandis, S. N., Poulain, L., Schlag, P., Sellegri, K., Swietlicki, E.,
224 Tiitta, P., Vermeulen, A., Wahner, A., Worsnop, D., and Wu, H.-C.: Ubiquity of organic nitrates
225 from nighttime chemistry in the European submicron aerosol, *Geophysical Research Letters*, 43,
226 7735-7744, <https://doi.org/doi:10.1002/2016GL069239>, 2016.

227 Kirchstetter, T. W., Novakov, T., and Hobbs, P. V.: Evidence that the spectral dependence of light
228 absorption by aerosols is affected by organic carbon, *Journal of Geophysical Research-*
229 *Atmospheres*, 109, D21208, <https://doi.org/10.1029/2004JD004999>, 2004.

230 Koss, A. R., Sekimoto, K., Gilman, J. B., Selimovic, V., Coggon, M. M., Zarzana, K. J., Yuan, B.,
231 Lerner, B. M., Brown, S. S., Jimenez, J. L., Krechmer, J., Roberts, J. M., Warneke, C., Yokelson,
232 R. J., and de Gouw, J.: Non-methane organic gas emissions from biomass burning: identification,
233 quantification, and emission factors from PTR-ToF during the FIREX 2016 laboratory experiment,
234 *Atmos. Chem. Phys.*, 18, 3299-3319, <https://doi.org/10.5194/acp-18-3299-2018>, 2018.

235 Lack, D. A., Langridge, J., Bahreni, R., Cappa, C. D., Middlebrook, A., and Schwarz, J. P.: Brown
236 Carbon and Internal Mixing in Biomass Burning Particles, *PNAS*, 10, 14802-14807,
237 <https://doi.org/10.1073/pnas.1206575109>, 2012a.

238 Lack, D. A., Richardson, M. S., Law, D., Langridge, J. M., Cappa, C. D., McLaughlin, R. J., and
239 Murphy, D. M.: Aircraft Instrument for Comprehensive Characterization of Aerosol Optical
240 Properties, Part 2: Black and Brown Carbon Absorption and Absorption Enhancement Measured
241 with Photo Acoustic Spectroscopy, *Aerosol Science and Technology*, 46, 555-568,
242 <https://doi.org/10.1080/02786826.2011.645955>, 2012b.

243 Langridge, J. M., Richardson, M. S., Lack, D., Law, D., and Murphy, D. M.: Aircraft Instrument
244 for Comprehensive Characterization of Aerosol Optical Properties, Part I: Wavelength-Dependent
245 Optical Extinction and Its Relative Humidity Dependence Measured Using Cavity Ringdown
246 Spectroscopy, *Aerosol Science and Technology*, 45, 1305-1318,
247 <https://doi.org/10.1080/02786826.2011.592745>, 2011.

248 Lim, C. Y., Hagan, D. H., Coggon, M. M., Koss, A. R., Sekimoto, K., De Gouw, J., Warneke, C.,
249 Cappa, C. D., and Kroll, J. H.: Secondary organic aerosol formation from biomass burning
250 emissions, *Atmos. Chem. Phys. Discuss.*, <https://doi.org/10.5194/acp-2019-326>, 2019.

251 Metcalf, A. R., Loza, C. L., Coggon, M. M., Craven, J. S., Jonsson, H. H., Flagan, R. C., and
252 Seinfeld, J. H.: Secondary Organic Aerosol Coating Formation and Evaporation: Chamber Studies
253 Using Black Carbon Seed Aerosol and the Single-Particle Soot Photometer, *Aerosol Sci. Technol.*,
254 47, 326-347, <https://doi.org/10.1080/02786826.2012.750712>, 2013.

255 Onasch, T. B., Trimborn, A. M., Fortner, E. C., Jayne, J. T., Kok, G. L., Williams, L. R.,
256 Davidovits, P., and Worsnop, D. R.: Soot Particle Aerosol Mass Spectrometer: Development,
257 Validation and Initial Application, *Aerosol Science and Technology*, 46, 804-817,
258 <https://doi.org/10.1080/02786826.2012.663948>, 2012.

259 Phillips, S. M., and Smith, G. D.: Spectroscopic comparison of water- and methanol-soluble brown
260 carbon particulate matter, *Aerosol Science and Technology*, 51, 1113-1121,
261 <https://doi.org/10.1080/02786826.2017.1334109>, 2017.

262 Qin, Y. M., Tan, H. B., Li, Y. J., Li, Z. J., Schurman, M. I., Liu, L., Wu, C., and Chan, C. K.:
263 Chemical characteristics of brown carbon in atmospheric particles at a suburban site near
264 Guangzhou, China, *Atmos. Chem. Phys.*, 18, 16409-16418, [https://doi.org/10.5194/acp-18-16409-](https://doi.org/10.5194/acp-18-16409-2018)
265 [2018](https://doi.org/10.5194/acp-18-16409-2018), 2018.

266 Saleh, R., Hennigan, C. J., McMeeking, G. R., Chuang, W. K., Robinson, E. S., Coe, H., Donahue,
267 N. M., and Robinson, A. L.: Absorptivity of brown carbon in fresh and photo-chemically aged
268 biomass-burning emissions, *Atmospheric Chemistry and Physics*, 13, 7683-7693,
269 <https://doi.org/10.5194/acp-13-7683-2013>, 2013.

270 Sekimoto, K., Koss, A. R., Gilman, J. B., Selimovic, V., Coggon, M. M., Zarzana, K. J., Yuan, B.,
271 Lerner, B. M., Brown, S. S., Warneke, C., Yokelson, R. J., Roberts, J. M., and de Gouw, J.: High-
272 and low-temperature pyrolysis profiles describe volatile organic compound emissions from
273 western US wildfire fuels, *Atmos. Chem. Phys.*, 18, 9263-9281, [https://doi.org/10.5194/acp-18-](https://doi.org/10.5194/acp-18-9263-2018)
274 [9263-2018](https://doi.org/10.5194/acp-18-9263-2018), 2018.

275 Sengupta, D., Samburova, V., Bhattarai, C., Kirillova, E., Mazzoleni, L., Iaukea-Lum, M., Watts,
276 A., Moosmüller, H., and Khlystov, A.: Light absorption by polar and non-polar aerosol compounds
277 from laboratory biomass combustion, *Atmos. Chem. Phys.*, 18, 10849-10867,
278 <https://doi.org/10.5194/acp-18-10849-2018>, 2018.

279 Shamjad, P. M., Tripathi, S. N., Thamban, N. M., and Vreeland, H.: Refractive Index and
280 Absorption Attribution of Highly Absorbing Brown Carbon Aerosols from an Urban Indian City-
281 Kanpur, *Scientific Reports*, 6, 37735, <https://doi.org/10.1038/srep37735>, 2016.

282 Sumlin, B. J., Pandey, A., Walker, M. J., Pattison, R. S., Williams, B. J., and Chakrabarty, R. K.:
283 Atmospheric Photooxidation Diminishes Light Absorption by Primary Brown Carbon Aerosol
284 from Biomass Burning, *Environmental Science & Technology Letters*, 4, 540-545,
285 <https://doi.org/10.1021/acs.estlett.7b00393>, 2017.

286 Sumlin, B. J., Heinson, Y. W., Shetty, N., Pandey, A., Pattison, R. S., Baker, S., Hao, W. M., and
287 Chakrabarty, R. K.: UV–Vis–IR spectral complex refractive indices and optical properties of
288 brown carbon aerosol from biomass burning, *Journal of Quantitative Spectroscopy and Radiative*
289 *Transfer*, 206, 392-398, <https://doi.org/10.1016/j.jqsrt.2017.12.009>, 2018.

290 Wandinger, Ulla, Müller, Detlef, Böckmann, Christine, Althausen, Dietrich, Matthias, Volker,
291 Bösenberg, Jens, Weiß, Volker, Fiebig, Markus, Wendisch, Manfred, Stohl, Andreas, and
292 Ansmann, A.: Optical and microphysical characterization of biomass- burning and industrial-
293 pollution aerosols from- multiwavelength lidar and aircraft measurements, *Journal of Geophysical*
294 *Research: Atmospheres*, 107, LAC 7-1-LAC 7-20, <https://doi.org/doi:10.1029/2000JD000202>,
295 2002.

296 Washenfelder, R. A., Attwood, A. R., Brock, C. A., Guo, H., Xu, L., Weber, R. J., Ng, N. L., Allen,
297 H. M., Ayres, B. R., Baumann, K., Cohen, R. C., Draper, D. C., Duffey, K. C., Edgerton, E., Fry,
298 J. L., Hu, W. W., Jimenez, J. L., Palm, B. B., Romer, P., Stone, E. A., Wooldridge, P. J., and
299 Brown, S. S.: Biomass burning dominates brown carbon absorption in the rural southeastern
300 United States, *Geophysical Research Letters*, 42, 653-664,
301 <https://doi.org/10.1002/2014GL062444>, 2015.

302 Xie, M., Hays, M. D., and Holder, A. L.: Light-absorbing organic carbon from prescribed and
303 laboratory biomass burning and gasoline vehicle emissions, *Scientific Reports*, 7, 7318,
304 <https://doi.org/10.1038/s41598-017-06981-8>, 2017.

305 Yang, M., Howell, S. G., Zhuang, J., and Huebert, B. J.: Attribution of aerosol light absorption to
306 black carbon, brown carbon, and dust in China – interpretations of atmospheric measurements
307 during EAST-AIRE, *Atmospheric Chemistry and Physics*, 9, 2035-2050,
308 <https://doi.org/10.5194/acp-9-2035-2009>, 2009.

309 Zhang, X., Kim, H., Parworth, C., Young, D. E., Zhang, Q., Metcalf, A. R., and Cappa, C. D.:
310 Optical Properties of Wintertime Aerosols from Residential Wood Burning in Fresno, CA: Results
311 from DISCOVER-AQ 2013, *Environmental Science & Technology*, 50, 1681-1690,
312 <https://doi.org/10.1021/acs.est.5b04134>, 2016.

313